Article

Study on the Vibration Characteristics of Rape Plants Based on High-Speed Photography and Image Recognition

Guangchao Zhan [1,2], Lina Ma [1,2], Wangyuan Zong [1,2,*], Wei Liu [1,2], Dinglin Deng [1,2] and Guodang Lian [1,2]

1   College of Engineering, Huazhong Agricultural University, Wuhan 430070, China;
    guangchaozhan@webmail.hzau.edu.cn (G.Z.); sunnylina@mail.hzau.edu.cn (L.M.);
    liuwei1@webmail.hzau.edu.cn (W.L.); ddl@webmail.hzau.edu.cn (D.D.); lgd929@webmail.hzau.edu.cn (G.L.)
2   Key Laboratory of Agricultural Equipment in Mid-lower Yangtze River, Ministry of Agriculture and Rural Affairs,
    Wuhan 430070, China
*   Correspondence: zwy@mail.hzau.edu.cn; Tel.: +86-131-0062-6908

Abstract: The transmission characteristics of the vibration excitation of rape plants are of great significance to the study of the harvesting loss and threshing mechanism of rape during harvesting. Aiming to examine the problem that the existing vibration measurement method cannot be well adapted to the vibration measurement of small plants such as rape, this article proposes a vibration measurement method based on high-speed photography and image recognition and uses this measurement method to study the vibration characteristics of rape plants in the three states, i.e., sweep frequency, standing frequency, and free attenuation, with a default hydraulic shaker. The results showed that the average measurement error of the vibration amplitude of this method was 0.0068 mm, and the relative measurement error of the amplitude at 20 Hz was 0.45%, which met the test requirements. Based on this measurement method, a sweep frequency test of rape plants was carried out. It was found that the first-order and second-order vibration modes of rape plants were concentrated in the first 15 Hz. The resonance range of rape plants mainly occurred at 6–7 Hz and 11–12 Hz. The standing frequency vibration test showed that rape plants had strong resonance at 6 Hz and 11 Hz, and grain falling was 1.192% and 0.992%, respectively, which was greater than those of other frequencies. The free attenuation vibration of the rape plant showed that the average attenuation coefficients of the mark points on the lateral branch at 20 cm, 30 cm, and 40 cm from the branch node were 0.542, 0.475, and 0.441, respectively, and the attenuation coefficient decreased as the distance between the mark point and the branch node increased. The amplitude attenuation coefficient of the main branch had little difference, and the average value was 0.797. This research can provide some reference for exploring the threshing mechanism of the rape drum and optimizing the header structure and parameters.

Keywords: rape plant; vibration characteristics; high-speed photography; image recognition

1. Introduction

Rape plants comprise an important oil crop worldwide, with a planting area of 70 million hectares in China [1–3]. A long-endured problem in rape production is the enormous loss generated with mechanized harvesting. The main causes for this problem are that the plant is multibranched and that the rape pods located in the upper and lower parts of the rape plant have different maturity levels [4–7]. The fragile pods located in the upper layer of the rape plant have high maturity levels and are more prone to cracking with the effects of reel tine and the vibration collision force of vertical cutters, resulting in grain loss during harvest [8–11]. The sturdy pods located in the lower layer of the rape plant have low maturity levels and are difficult to thresh, which increases the threshing loss rate [12]. Therefore, it is urgent to study the mechanism of seed abscission during rape harvest to determine the relevant factors affecting rape pod seed falling, which provides a reference for optimizing rape combine harvesters.

Many studies have been conducted to decrease rape seed loss during harvest. In particular, the physical characteristics of rape plants were studied, including improving rape varieties to select rape varieties suitable for mechanized harvest and selecting an appropriate harvest time to reduce the loss of rape seeds [8,13,14]. Moreover, some scholars have studied the harvesting methods of rape. First, the rape is cut down and laid in the field for drying, and then the dried rape is threshed through a pickup device. This method allows rape to be fully mature and easy to thresh, but there is inevitably a serious problem of grain loss in the process of picking and threshing [15]. Additionally, the vibration of all parts of the combine harvesters is decreased to reduce the force of the header on the plant, reducing grain loss in the harvest process [16–19]. The above methods require many experiments and continuous optimization of the device, which is time-consuming and laborious, and the process of grain falling is not explained fundamentally. Studying the transmission characteristics of dynamic excitation in rape plants and clarifying the process of grain falling will be a major future research trend. Research on plant vibration mainly focuses on vibration fruit picking. For example, Yang Huimin et al. [20,21] used ANSYS software to conduct finite element modeling analysis on apricot trees and analyzed the influence of different vibration characteristic parameters on apricot vibration detection points through experiments. He Miao et al. [22,23] determined an optimal parameter combination of fruit pedicle separation by studying the fruit pedicle separation conditions and the dynamic transfer characteristics between *Lycium barbarum* branches in the process of vibration harvesting machinery. Wang Qirui et al. [24–26] proposed a dynamic simulation model considering the vibration response characteristics of flexible crop stems and studied the dynamic response characteristics of crop stems. In summary, the main research ideas of plant vibration characteristics include plant modeling and simulation and experimental research on the transmission process of excitation signals in plants with the help of acceleration sensors [27], but the premise of this method is that the installed sensor must ignore the influence on the vibration frequency of the measured object. Therefore, the method of installing sensors on rape plants is not applicable.

In this paper, a noncontact measurement method is proposed. First, the vibration-state images of the characteristic points on rape plants were collected by a high-speed camera [28]. Then, after batch processing, such as threshold segmentation, denoising, and feature point center coordinate extraction, the motion trajectory data of the feature points were obtained. Finally, the accuracy of the measurement method was verified with a hydraulic vibration shaker. Using this measurement method, the sweep frequency test, standing frequency test, and free attenuation vibration test of rape plants were carried out with a hydraulic vibration shaker. Through this experiment, the resonance range of the rape plant and the corresponding vibration grain falling during plant resonance were obtained, and the attenuation coefficient of the amplitude in the rape plant was also determined. This study can provide a theoretical reference for the mechanized harvesting of rape.

2. Materials and Methods

2.1. Stress Analysis of Rape during Combined Harvest

In the process of rape combined harvest, grain loss mainly occurs in the falling grain loss caused by the reel fingers and the threshing loss caused by the insufficient separation of rape threshing. Figures 1 and 2 show the force analyses of the actions of the reel finger and threshing nail teeth on the rape plant, respectively.

In Figure 1, the rape plant at point B is moved by the reel finger, where F_r is the force of the reel finger on the plant, F_q is the elastic force of the stalk against deformation, and the direction is perpendicular to the lateral branches. F_σ is the traction along the stalk direction, then

$$\overrightarrow{F_q} + \overrightarrow{F_\sigma} = -\overrightarrow{F_r} \tag{1}$$
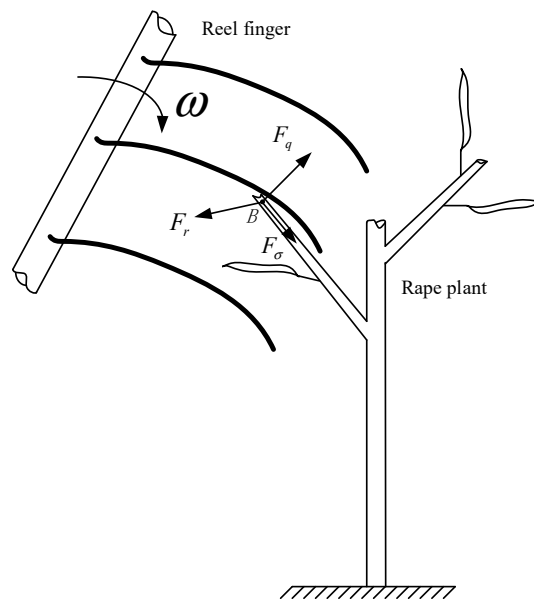
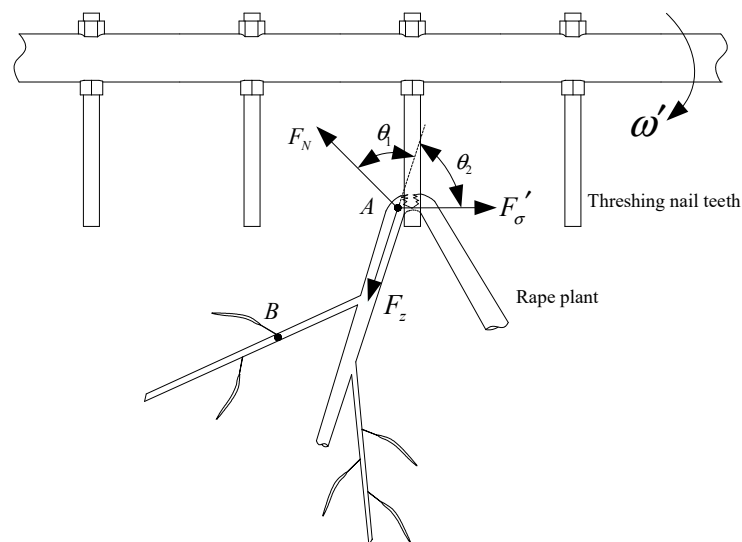**Figure 1.** Analysis of shifting force on rape plant by reel finger.

Figure 2. Analysis of hitting force on rape plant by threshing nail teeth.

In Figure 2, the rape material fed into the threshing drum falls under the action of gravity and collides with the threshing nail teeth in the falling process. The threshing nail teeth are installed on the teeth rod and rotate around the center of the drum at speed ω. Due to the action of stalk epidermal fiber, the rape stalk will not be broken immediately after being impacted by the nail teeth. The stress analysis was carried out at the "A" point of the main stalk of rape. Point A is subjected to the tensile stress, F_σ', of the partially broken stalk, the impact force, F_N, of the threshing nail teeth on the stalk, and the resistance, F_Z, along the moving direction of the stalk. The mechanical force analysis of the rape stalk in the direction of the moving speed and vertical speed can be expressed as follows:

$$F_N \sin \theta_1 = F_q \sin \theta_2 \tag{2}$$

$$F_N \cos \theta_1 + F_q \cos \theta_2 - F_Z = ma \tag{3}$$

where m is the equivalent mass below point A, kg, and a is the acceleration of stem movement, m/s^2.

The analyses of the actions of the reel finger and threshing nail teeth on the rape plant show that the common feature of dynamic excitation in the process of rape plant harvest is local force, and the parts without collision will also be affected by the dynamic excitation of the collision point.

In Figure 2, taking branch *AB* as the research object, *A* is the dynamic excitation contact point, and the part above point *B* is equivalent to the whole block with mass *m*. The part between points *A* and *B* can be equivalent to the spring damping model [29], as shown in Figure 3. The coordinate X downward is selected as positive, and the stress analysis on the position of point *B* is conducted. Due to the complex stress in the process of rape harvest, the stress in the direction of gravity is only analyzed here, then the force acting on point *B* is as follows: gravity, *F*, acting on point *B*, restoring force of spring $k(\Delta_{st} + x)$, which is related to the bending strength of the stalk, inertia force, $\frac{F}{g}x''$, interference force, $F_d \sin \omega t$, which is related to forced vibration response, and damping force, F_0, which includes air damping and internal friction of straw. The damping force is usually assumed to be proportional to the speed as follows: $F_0 = cx'$, where *c* is the proportional constant.
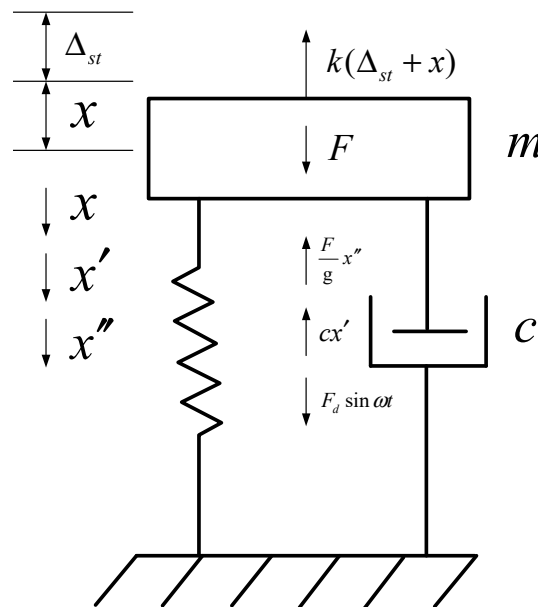

Figure 3. Simplified stress analysis model.

Thus, the motion equation of the rape plant can be obtained:

$$\frac{F}{g}x'' + cx' + k(\Delta_{st} + x) - F - F_d \sin \omega t = 0 \tag{4}$$

By simplifying the above formula, and because $k\Delta_{st} = F$,

$$x'' + \frac{gc}{F}x' + \frac{kg}{F}x = \frac{F_d g}{F} \sin \omega t \tag{5}$$

The natural frequency of the system ω_0 is as follows:

$$\omega_0 = \sqrt{\frac{g}{\Delta_{st}}} = \sqrt{\frac{kg}{F}} \tag{6}$$

The following variables are introduced:

$$\delta = \frac{gc}{2F} \tag{7}$$

where δ is the damping coefficient; then, Equation (5) can be simplified as

$$x'' + 2\delta \cdot x' + \omega_0^2 \cdot x = \frac{F_d g}{F} \sin \omega t \tag{8}$$

In the case of small damping, $\delta < \omega_0$, the general solution of the above equation can be calculated:

$$x = Ae^{-\delta \cdot t} \sin\left(\sqrt{\omega_0^2 - \delta^2}t + \alpha\right) + B\sin(\omega t + \varepsilon) \tag{9}$$

The first part of the formula is the attenuation vibration, which decreases rapidly with increasing time and ultimately disappears. The second part is forced vibration. After the first part disappears, only forced vibration remains, and the equation can be simplified as: $x = B\sin(\omega t + \varepsilon)$. In the above formula:

$$B = \frac{F_d g}{F\omega_0^2 \sqrt{\left[1 - \left(\frac{\omega}{\omega_0}\right)^2\right]^2 + 4\left(\frac{\delta}{\omega_0}\right)^2\left(\frac{\omega}{\omega_0}\right)^2}} \tag{10}$$

$$\varepsilon = \arctan\frac{2\delta\omega}{\omega_0^2 - \omega^2} \tag{11}$$

The theoretical analysis shows that the amplitude of the forced vibration of the stalk is related to the natural frequency, damping coefficient, quality, and other factors of the stem itself. The natural frequency can determine when the vibration amplitude of the rape plant is the strongest and obtain the best frequency of grain vibration and grain falling, which can effectively guide the improvement of the device. The damping coefficient is mainly determined by the attenuation coefficient of the amplitude in the plant. By measuring the attenuation coefficient of the amplitude in each part of the rape plant, the optimal position of the harvesting device with respect to the plant can be determined, and the critical condition for the force acting on the stem to be transmitted to the pod to cause grain falling can be obtained.

2.2. Test Materials and Method

The materials used in the experiments were collected and picked from the experimental farm of Huazhong Agricultural University. The variety planted on the farm was "Huayouza 62", a winter *Brassica napus* variety developed by the researchers of Huazhong Agricultural University in 2011 and now widely planted in central China. The average water content of the main stalk was 68.94%.

In this experiment, whole rapeseed plants, which were pest-free and well-grown, were cut and collected from six randomly chosen patches of the experimental farm. First, vibrations of different frequencies were generated using a hydraulic vibration shaker. The frequency range within which the plants showed severe vibrations was determined by a sweep frequency test. Six rape plants were measured in each group, and measurements were repeated three times. Then, tests of fixed frequencies were performed. For each frequency, the vibration lasted 120 s in one test. The ratio of the drop seed weight to the whole rape seed weight was recorded, the test was repeated three times, and the average value was recorded. Finally, the rape plant was fixed on a shaking table, and a horizontal offset was applied to the lateral branches of the rape plant. The attenuation process of the swing amplitude was recorded by high-speed photography. To avoid interference from nearby stems, only one main stem was clamped on the shaker in each test. During the tests, the movements of the plants were recorded at a high speed, as shown in Figure 4.
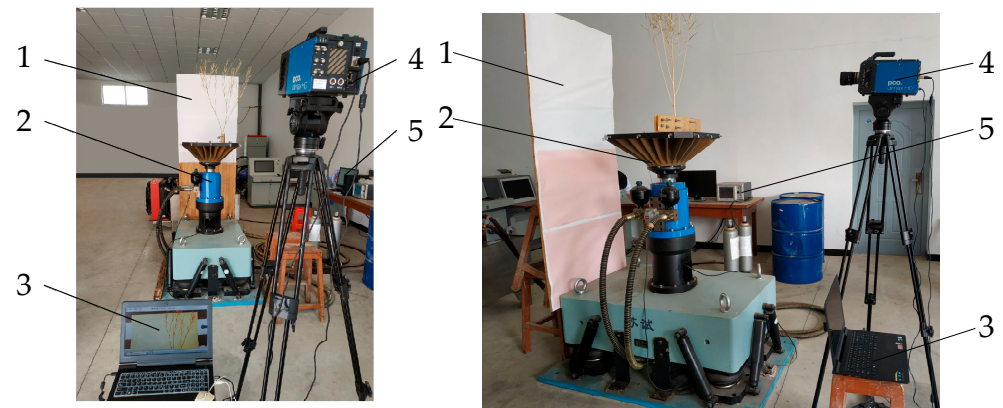
Figure 4. Experimental setup of rape plant vibration measurements: 1—background paper; 2—hydraulic shaker; 3—computer; 4—high-speed camera; 5—hydraulic console.

The equipment used in the test included a moisture analyzer (model MB45, OHAUS Corporation, Switzerland), high-speed photography system (PCO.dimax HD, PCO AG, Germany), hydraulic vibration shaker (model ES-3, Sushi Testing Instrument, China), marking pen, white background plate, scissors, and a tape measure. The parameters of the equipment are shown in Table 1.

Table 1. Parameters of equipment used in the noncontact measurement method.

Equipment	Parameter	Parameter value
PCO.dimax HD	Resolving power	2 megapixels (1920 × 1440)
	Shooting speed	1~2128 frames/s (adjustable)
	Shutter speed	1.5 μs~1 s (adjustable)
	Spectral response range	290~1100 nm
Hydraulic vibration shaker	Frequency range	0.1~160 Hz
	Direction of vibration	vertical
	Maximum vertical acceleration	40 m/s^2
	Maximum sinusoidal force	30 KN
	Displacement range	±100 mm

2.3. Measurement Method of Rape Plant Vibration

2.3.1. Image Acquisition

The prepared rape plant sample was clamped on the fixture of a hydraulic vibration testbed, and the vibration signal was applied to the rape plant by the hydraulic vibration testbed. In the process of rape plant vibration, the vibration state of the rape plant was recorded with a high-speed camera, and the sampling frequency of high-speed photography is 200 Hz.

During the test, the bottom of the rape stalk was clamped and fixed on the vibration testbed. High-speed photography and the marking points on the rape plants remained at the same level. Since the applied vibration signal was in the vertical direction, the vibration amplitude in the vertical direction of the plant was the largest, so only the vertical amplitude of the marked points on each pod was recorded.

2.3.2. Feature Point Coordinate Recognition

In this paper, MATLAB software (GRALL07b, R2007b GR KIT WIN-MAC-UNIX, Natick, MA, USA) was used to batch process the pictures recorded by high-speed photography to measure the vibration at the marked points of the rape plants. The specific process included image clipping, image threshold segmentation, image filtering, and mark point coordinate extraction. The specific operations were as follows:

(1) First, the pictures taken by high-speed photography were segmented. Because the position of high-speed photography was fixed and the rape plant was fixed on the fixture of the vibration testbed, the parts other than the plant mark points may interfere with the recognition of the feature points. Therefore, the parts other than the image mark points were segmented to obtain images containing only the mark points.

(2) Threshold segmentation and filtering were performed on the segmented images. In the experiment, a black marker was used to mark the plant, and there were black spots on various parts of the plant that interfered with the marked points. Therefore, the binarization process contained local noise, and the images needed to be filtered. Because the local noise was generally less than the marked points, according to the size of the marked points, the binary image was processed by corrosion expansion in this paper. While corroding the local noise, the image marking points were expanded to eliminate the noise as much as possible and ensure that the size and center position of the marking points remained unchanged. Images of the rapeseed plant marked feature points and threshold segmentation are shown in Figure 5.
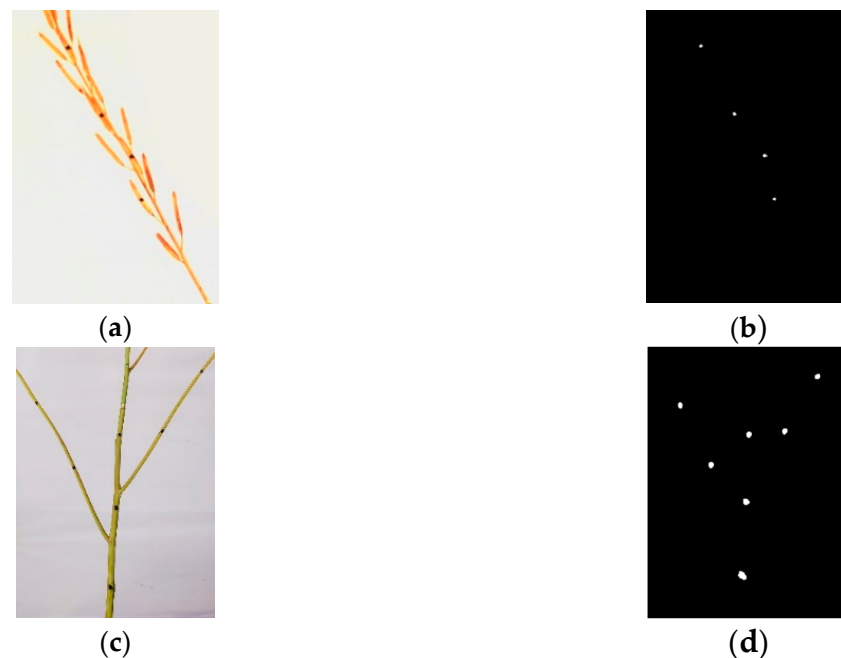

(**a**)   (**b**)

(**c**)   (**d**)

Figure 5. Figures of rape plant's measurement point marks and threshold segmentation. (**a**) Image of rape pods marked feature points. (**b**) Threshold segmentation image of rape pods. (**c**) Image of rape branches marked feature points. (**d**) Threshold segmentation image of rape branches.

(3) Mark point coordinate extraction: The processed pictures were named with digital serial numbers and saved in the same folder. The pictures were exported in batches through MATLAB programming, and the center coordinates of the marked points in the pictures were solved. Thus, the displacement change of the marked point was $A_{(t)}$. At this time, the displacement signal was not the vibration signal of the feature points but the amplitude change of the feature points, and the vibration signal of the marked points was $X_{(t)}$:

$$X_{(t)} = \mu\left(A_{(t)} - A_0\right) \tag{12}$$

where A_0 is the offset of the center point when the mark point fluctuates up and down, and μ is the ratio of the amplitude of feature points on the picture to the actual amplitude of feature points.

2.3.3. Measurement Accuracy and Feasibility Analysis

At present, the measurement of vibration is mainly based on contact sensors, and few scholars measure it based on high-speed photography and image recognition. The accuracy and effectiveness of this method need to be verified. This study marked a point on the fixture of the vibration testbed, provided a sinusoidal signal to the hydraulic testbed, measured the signal with the help of high-speed photography and image recognition technology, and compared the measured signal with the actual signal to verify the effectiveness and accuracy of this method. The measurement accuracies of the two sinusoidal signals at 20 Hz and 60 Hz are shown in Table 2.

Table 2. Error analysis table of vibration signals.

Signal	20 Hz		60 Hz	
Numerical Value	Theoretical Value	Measured Value	Theoretical Value	Measured Value
Period/T (s)	0.05	0.0500	0.0167	0.0167
Frequency (Hz)	20	20.0000	60	59.8802
Velocity (m/s)	0.1592	0.1600	0.0531	0.0559
Acceleration (m/s^2)	20	20.0960	20	21.1122
Amplitude (mm)	1.2678	1.2735	0.1409	0.1487
Amplitude error (mm)	0.0057		0.0078	
Amplitude relative error (%)	0.45		5.54	

Table 2 shows that the test method is feasible. The average measurement error of the vibration amplitude was 0.0068 mm. The relative measurement error of the signal amplitude was only 0.45% at 20 Hz and 5.54% at 60 Hz. The error increased at higher frequencies, mainly due to the acceleration of the sinusoidal signal $a = (2\pi f)^2 d$, where f is the frequency and d is the stroke (twice the amplitude); when the acceleration, a, was certain, the amplitude decreased with increasing frequency, and the relative error was $\delta = \Delta A/A$. When the value of A remained unchanged, the amplitude decreased, and the relative error increased. During the test, only the vibration characteristics of rape plants in the first and second order were studied, so this measurement method is feasible for studying the vibration characteristics of rape plants.

3. Results and Discussion

3.1. Sweep Frequency Vibration Test of the Rape Plant

First, the console was preloaded to determine whether the hydraulic vibration shaker could complete the frequency sweep. To avoid the overload of the hydraulic vibration shaker, it started to sweep the frequency with a fixed amplitude when the frequency sweep signal of the hydraulic vibration shaker reached the preset amplitude. Then, the hydraulic vibration shaker was started, to apply the vibration signal to the rape plant, and the sweep frequency measurement signal as shown in Figure 6. The real-time vibration signal of the hydraulic vibration shaker as shown in Figure 6a. The vibration signal of the rape plant can be obtained by subtracting the signal applied by the vibration testbed from the measured signal. The measured signals of the main and lateral branches are shown in Figure 6b,c.

The amplitude fluctuated obviously at 7.150 s, 10.735 s, 16.645 s, and 18.570 s, as shown in Figure 6b. Since the data sampling frequency set by the high-speed camera was 200 Hz, it can be concluded that the time interval between the two data points was 0.005 s. Therefore, the frequency at the resonance point can be obtained by combining the number of measuring points in the vibration cycle where the signal peak point is located. The corresponding frequencies at each resonance point can be calculated as 3.64 Hz, 5.41 Hz, 11.11 Hz, and 14.29 Hz. The main branch had a maximum amplitude at a frequency of 14.29 Hz, and the maximum amplitude was 2.347 mm. Similarly, the lateral branches had a maximum amplitude at a frequency of 11.11 Hz, and the maximum amplitude was 6.922 mm, as shown in Figure 6c.
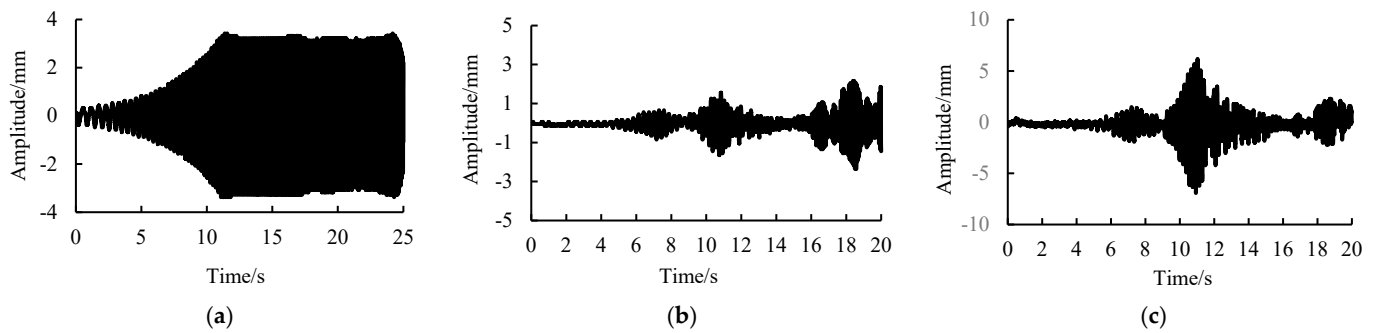
Figure 6. Sweep frequency measurement signal. (**a**) Frequency sweep signal of vibration bench. (**b**) Vibration signals of main branch. (**c**) Vibration signals of lateral branches.

Through the frequency sweep test, it was found that there were multiple resonance points in the frequency range of 1–15 Hz. The maximum deformation of plant vibration was usually in the first and second order. Therefore, a frequency sweep test was carried out on 18 rape plants, and the maximum amplitudes of the first and second peaks of the rape plants at 1–15 Hz were recorded. The frequency distribution range corresponding to the vibration peak point of the rape plant is shown in Figure 7. The resonance of rape plants mainly occurred at 6–7 Hz and 11–12 Hz.
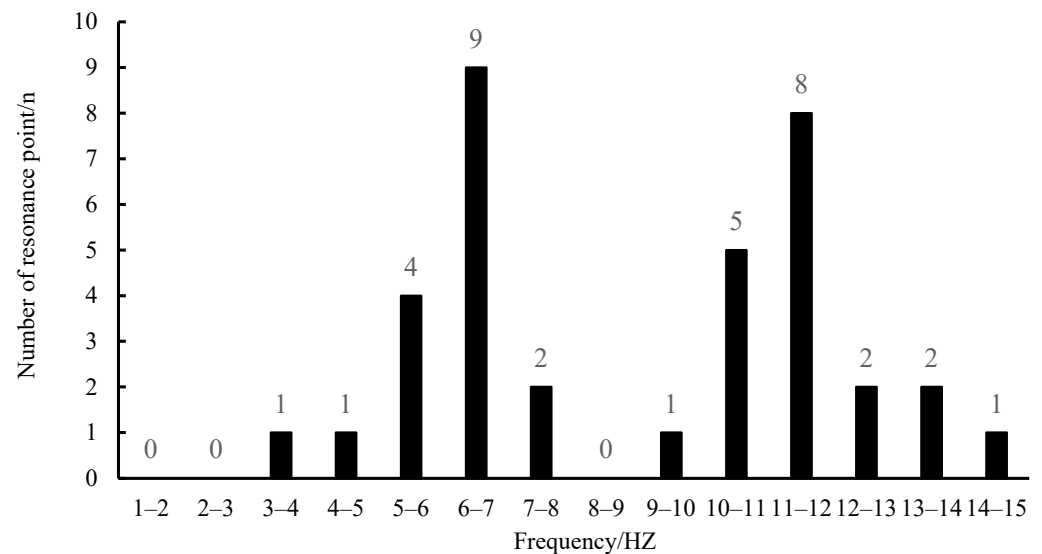

Figure 7. Frequency distribution range corresponding to the vibration peak point of the rape plant.

3.2. Sweep Frequency Vibration Test of the Rape Plant

To study the rapeseed falling of the rape plant at different frequencies, a standing frequency vibration test was carried out for the rapeseed-falling characteristics of the rape plant at various frequencies of 1~15 Hz. During the test, the vibration acceleration is 10 m/s^2. The maximum vibration grain falling of the rape plant was 1.19% at 6 Hz, followed by 0.99% at 11 Hz, which was greater than other frequencies, as shown in Figure 8. When developing the header, the vibration frequency of the header and the reeling frequency of the reel should be selected to avoid the resonance frequency of the rape plant, which can effectively reduce the serious problem of grain loss in the process of rape combined harvest.
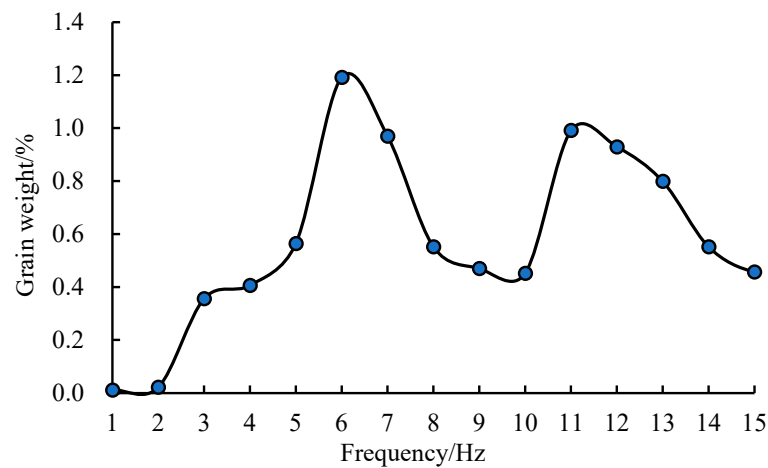
Figure 8. Vibration seed falling of rape plants under different frequencies.

3.3. Sweep Frequency Vibration Test of the Rape Plant

The vibration response of the rape plant will be transmitted from the stress point to the rape pod during rape harvest. In the process of vibration response transmission, the main factor affecting energy dissipation is the material damping of the rape plant itself. Therefore, determining the transmission characteristics of the vibration response in a rape plant is of great significance to clarify the threshing mechanism of rape.

During the experiment, taking the first branch node as the coordinate, points 20 cm, 30 cm, and 40 cm away from the node on the lateral branch and main branch were marked. The lateral branches of the rape plant were shifted by 80 mm. While loosening the plant, the attenuation process of the swing amplitude of the lateral branches of the rape plant was recorded by high-speed photography. The attenuation signal of the rape plant was obtained through later image processing, as shown in Figure 9.
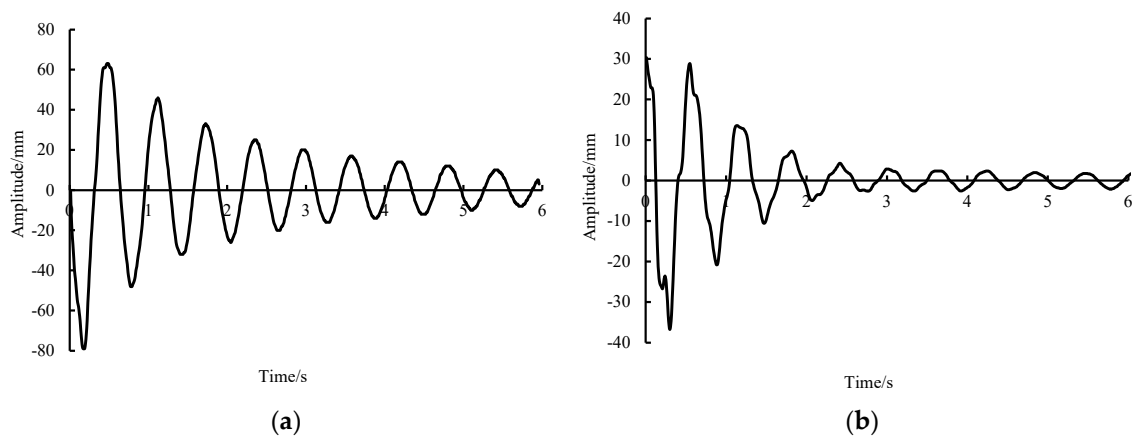

Figure 9. Damped free vibration signal of the rape plant. (**a**) Lateral branch. (**b**) Main branch.

According to the formula of exponential attenuation of amplitude [30]:

$$A(\tau) = A_0 \cdot e^{-\sigma \cdot \tau} \tag{13}$$

where A_0 is the initial amplitude and σ is the attenuation coefficient.

The exponential function was used to fit all peak points to obtain the exponential attenuation function of amplitude with time. The value of each peak point was logarithmically fitted, and the fitting degree was 0.97, as shown in Figure 10.
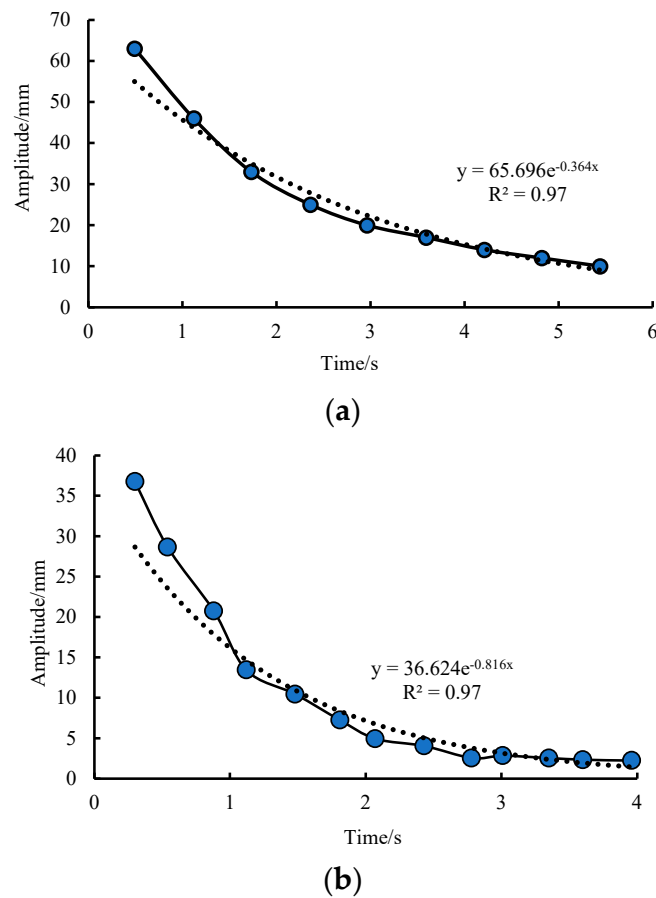
(**a**)

(**b**)

Figure 10. Fitting diagram of the attenuation function of each peak amplitude of the rape plant. (**a**) Lateral branch. (**b**) Main branch.

Taking the side branch as the node, the free attenuation vibrations of the marked points 20 cm, 30 cm, and 40 cm away from the node were recorded, and the attenuation coefficient of each point was measured. The attenuation coefficient of each point is shown in Figure 11.
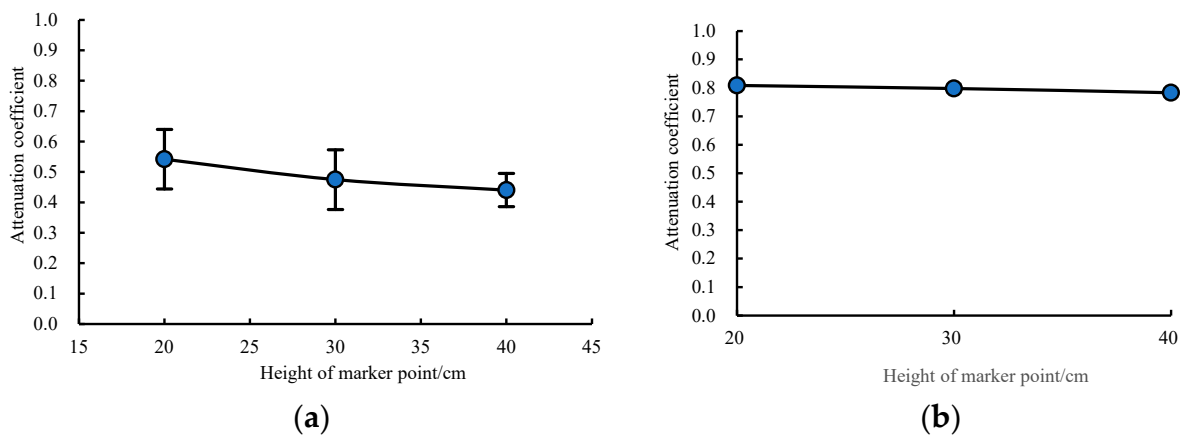

(**a**)

(**b**)

Figure 11. Attenuation coefficients at different mark points. (**a**) Lateral branch. (**b**) Main branch.

The average attenuation coefficients at 20 cm, 30 cm, and 40 cm from the main branch node on the side branch were 0.542, 0.475, and 0.441, respectively, as shown in Figure 11a. The attenuation coefficient decreases with the distance between the marker point and the

node, mainly because the farther the marker point of the rape lateral branch was from the node of the main branch, the thinner the diameter of the lateral branch at the marker point, the lower the degree of fibrosis, and the rape plant had weak resistance to deformation in the process of free attenuation vibration, so the attenuation coefficient of amplitude was smaller. The amplitude attenuation coefficient of the main branch showed little difference, and the average value was 0.797, as shown in Figure 11b.

4. Discussion

4.1. Universality Analysis of the Vibration Measurement Method

This paper presents a noncontact measurement method of rape plant vibration characteristics based on the combination of high-speed photography and image recognition. This measurement method is not only suitable for rapeseed plants but also for other crops. Compared with an acceleration sensor, which is limited by the transmission channel, this measurement method can mark multiple feature points and realize multipoint measurement at one time. However, because this measurement method is limited by the parameters of high-speed photography equipment, it cannot be measured for a long time. After a group of experiments are taken, the pictures need to be exported and saved, and then the vibration signal can be obtained after postprocessing. A set of data takes about 1 h to process. Subsequent research can integrate a high-speed camera with the coordinate recognition technology of feature points, which has good application prospects for the real-time measurement of plant vibration characteristics.

4.2. Effect of Different Frequencies on Vibration Modes of Rape Plants and Grain Falling

The frequency sweep test of rape plants showed that the resonance of rape plants mainly occurred at 6–7 Hz and 11–12 Hz. Because there are some differences among rape plants, the resonance point of the "Huayou Za 62" rape plant was preliminarily determined by statistical methods. Follow-up research can focus on the effects of different varieties of rape and water content on the vibration characteristics of rape. The standing frequency vibration test showed that the maximum vibration grain falling of the rape plant was 1.19% at 6 Hz, followed by 0.99% at 11 Hz. The experiment was carried out on the vibration testbed, and the rape plants will inevitably exhibit some losses in the process of manual harvesting and transportation. Therefore, the measured value of the rape vibration grain falling was slightly less than the actual value. During rape harvesting, avoid the resonance frequency of rape header at 6–7 Hz and 11–12 Hz, which can effectively reduce the grain falling loss. During rape threshing, optimal hitting frequency of threshing parts on rape are 6 Hz and 11 Hz for easier and more effective threshing.

4.3. Effects of Different Parts of the Rape Plant on the Vibration Amplitude Attenuation Coefficient

The average attenuation coefficients at 20 cm, 30 cm, and 40 cm from the main branch node on the side branch were 0.542, 0.475, and 0.441, respectively. The attenuation coefficient decreased with the distance between the marker point and the node, mainly because the farther the marker point of the rape lateral branch was from the node of the main branch, the thinner the diameter of the lateral branch at the marker point, the lower the degree of fibrosis, and thinner branch has weak resistance to deformation, so the attenuation coefficient of amplitude was smaller. The amplitude attenuation coefficient of the main branch showed little difference, and the average value was 0.797. The amplitude attenuation coefficient of the main branch was much greater than that of the side branch. During rape threshing, because the dynamic impact of threshing nail teeth on rape stalk is attenuated when it is transmitted from stalk to pods, making direct collision of threshing nail teeth with pods can make rape threshing easier and more effective. For example, reducing stalk feeding or adopting the stripping harvest method to increase impact probability of threshing nail teeth on pods.

5. Conclusions

(1) This paper presents a noncontact measurement method of rape plant vibration characteristics based on the combination of high-speed photography and image recognition. Through the analysis of the accuracy and feasibility of the measurement method, it can be seen that the average measurement error of the vibration amplitude of the test method was 0.0068 mm. With an increase in the vibration frequency, the relative error of the method decreased slightly, and the relative measurement error of the amplitude was 0.45% at 20 Hz.

(2) Through the frequency sweep test, it was found that there were multiple resonance points in the frequency range of 1–15 Hz. The maximum deformation of plant vibration is usually in the first and second order. The resonance of rape plants mainly occurred at 6–7 Hz and 11–12 Hz.

(3) The standing frequency vibration test of rape plants in the frequency range of 1~15 Hz showed that rape plants had resonance at 6 Hz and 11 Hz, and the vibration and grain falling were 1.192% and 0.992%, respectively, which was greater than those of other frequencies.

(4) The free attenuation vibration test of rape plants showed that the average attenuation coefficients of the marked points on the side branches at 20 cm, 30 cm, and 40 cm away from the main branch and side branch nodes were 0.542, 0.475, and 0.441, respectively. The attenuation coefficient decreased with increasing distance between the marked points and the nodes, and the attenuation coefficients of the marked points on the main branch showed little difference, with an average value of 0.797.

Institutional Review Board Statement: Not applicable.

Informed Consent Statement: Not applicable.

Data Availability Statement: The data presented in this study are available on demand from the first author at (guangchaozhan@webmail.hzau.edu.cn).

Conflicts of Interest: The authors declare no conflict of interest. The funder had no role in the design of the study; in the collection, analyses, or interpretation of data; in the writing of the manuscript, or in the decision to publish the results.

References

1. Hu, Y.; Gu, J.J.; Guo, J. Study on influencing factors and harvest mode of rape mechanized production. *J. Agric. Mech. Res.* **2020**, *42*, 179–182.
2. Cavalieri, A.; Harker, K.N.; Hall, L.M.; Willenborg, C.J.; Haile, T.A.; Shirtliffe, S.J.; Gulden, R.H. Evaluation of the Causes of On-Farm Harvest Losses in Canola in the Northern Great Plains. *Crop Sci.* **2016**, *56*, 2005–2015. [CrossRef]
3. Pahkala, K.; Sankari, H. Seed loss as a result of pod shatter in spring rape and spring turnip rape in Finland. *Agr. Food Sci. Finland* **2001**, *10*, 209–216. [CrossRef]
4. Pari, L.; Assirelli, A.; Suardi, A.; Civitarese, V.; Del Giudice, A.; Costa, C.; Santangelo, E. The harvest of oilseed rape (*Brassica napus* L.): The effective yield losses at on-farm scale in the Italian area. *Biomass Bioenergy* **2012**, *46*, 453–458. [CrossRef]
5. Qing, Y.R.; Li, Y.M.; Xu, L.Z.; Ma, Z.; Tan, X.L.; Wang, Z. Oilseed rape (*Brassica napus* L.) pod shatter resistance and its relationship with whole plant and pod characteristics. *Ind. Crops Prod.* **2021**, *166*, 113459. [CrossRef]
6. Li, Y.M.; Zhu, J.Q.; Xu, L.Z.; Zhao, Z. Experiment on strength of rapeseed pod dehiscence based on impending fracturing method. *Trans. CSAE* **2012**, *28*, 111–115.
7. Brace, D.M.; Farrent, J.W.; Morgan, C.L.; Child, R.D. Determining the oilseed rape pod strength needed to reduce seed loss due to pod shatter. *Biosyst. Eng.* **2002**, *81*, 179–184.

8. Qing, Y.R.; Li, Y.M.; Xu, L.Z.; Ma, Z. Screen oilseed rape (*Brassica napus*) suitable for low-loss mechanized harvesting. *Agriculture* **2021**, *11*, 504. [CrossRef]
9. Ma, L.N.; Wei, J.Y.; Huang, X.M.; Zong, W.Y.; Zhan, G.C. Analysis of harvesting losses of rapeseed caused by vibration of combine harvester header during field operation. *Trans. CSAM* **2020**, *51*, 141–145.
10. Hobson, R.N.; Bruce, D.M. Seed loss when cutting a standing crop of oilseed rape with two types of combine harvester header. *Biosyst. Eng.* **2002**, *81*, 281–286. [CrossRef]
11. Chai, X.Y.; Xu, L.Z.; Yan, C.; Liang, Z.W.; Ma, Z.; Li, Y.M. Design and test of cutting frequency follow-up adjusting device for vertical cutting knife of rapeseed cutting machine. *Trans. CASM* **2018**, *49*, 100–106.
12. Wang, G.; Guan, Z.H.; Mu, S.L.; Tang, Q.; Wu, C.Y. Optimization of operating parameter and structure for seed thresher device for rape combine harvester. *Trans. CSAE* **2017**, *33*, 52–57.
13. Wang, R.; Ripley, V.L.; Rakow, G.R. Pod shatter resistance evaluation in cultivars and breeding lines of Brassica napus, Brassica juncea and Sinapis Alba. *Plant Breed.* **2007**, *126*, 588–595. [CrossRef]
14. Luo, H.F.; Tang, C.Y.; Guan, C.Y.; Wu, M.L.; Xie, F.P.; Zhou, Y. Plant characteristic research on field rape based on mechanized harvesting adaptability. *Trans. CSAE* **2010**, *26*, 61–66.
15. Wu, C.Y.; Ding, W.M.; Shi, L.; Wang, L.Q.; Jin, C.Q. Response surface analysis of pickup losses in two-stage harvesting for rapeseed. *Trans. CSAM* **2011**, *42*, 89–93.
16. Ren, S.G.; Wu, M.L.; Xie, W.; Tang, S.Z. Oilseed rape harvest cutting impact stress wave and its propagation in the stalk. *Agro Food Ind. Hi-Tech* **2017**, *28*, 1493–1495.
17. Li, Y.; Xu, L.Z.; Gao, Z.P.; Lu, E.; Li, Y.M. Effect of vibration on rapeseed header loss and optimization of header farme. *Trans. ASABE* **2021**, *64*, 1247–1258. [CrossRef]
18. Ran, J.H.; Mu, S.L.; Li, H.T.; Guan, Z.H.; Tang, Q.; Wu, C.Y. Design and test of planet gear driver of reciprocating double-acting cutter for rapeseed combine harvester. *Trans. CSAE* **2020**, *36*, 17–25.
19. Ren, S.G.; Jiao, F.; Wu, M.L.; He, S.Z.; Tang, S.Z. Studies of United Harvest Machine Cutting System Structure Parameters on the Vibration Impact. *J. Agric. Mech. Res.* **2018**, *40*, 38–43.
20. Yang, H.M.; San, Y.L.; Chen, Y.F.; Wang, X.N.; Niu, C.H.; Hou, S.L. Influence of different vibration characteristic parameters on vibration response of apricot trees. *Trans. CSAE* **2019**, *35*, 10–16.
21. San, Y.L.; Yang, H.M.; Wang, X.N.; Guo, W.S.; Hou, S.L. Dynamic response analysis of apricot fruit dropping during vibration harvesting. *Trans. CSAE* **2018**, *34*, 68–75.
22. Wang, Y.L.; Chen, Y.; Han, B.; Chen, J. Research on laws of wolfberry dropping based on high-speed camera. *Trans. CSAE* **2018**, *40*, 166–170.
23. Zhao, J.; Tsuchikawa, S.; Ma, T.; Hu, G.R.; Chen, Y.; Wang, Z.W.; Chen, Q.Y.; Gao, Z.N.; Chen, J. Modal analysis and experiment of a lycium barbarum L. Shrub for efficient vibration harvesting of fruit. *Agriculture* **2021**, *11*, 519. [CrossRef]
24. Wang, Q.R.; Mao, H.P.; Li, Q.L. Simulation of vibration response of flexible crop stem based on discrete element method. *Trans. CSAM* **2020**, *51*, 138–144.
25. Fan, L.G.; Wang, C.Y.; Liu, M.X.; Luo, J.Q. Experimental study on the impact of vibration parameters on fruit trees. *J. Agric. Mech. Res.* **2016**, *38*, 171–174.
26. Liu, Z.L.; Wang, C.Y.; Wei, T.P.; Lv, M.L. The research of fruit trees dynamic characteristics with impact vibration. *Acta Agric. Univ. Jiangxiensis* **2016**, *4*, 495–499.
27. Ding, H.X.; Li, M.T.; Xue, Z.M. The test device design and vibration of main low order resonance frequency of picking mulberry. *J. Agric. Mech. Res.* **2017**, *39*, 159–164.
28. Chen, J.X.; Yue, D.P.; Feng, Z.K.; Ding, J.W.; Yao, B.Q.; Ye, T.X. Automatic recognition and measurement technology of tree trunk diameter. *Trans. CASM* **2016**, *47*, 349–353.
29. Ren, S.G.; Wu, M.L.; Xie, F.P.; Guan, C.Y. Study on viscoelastic properties of rapeseed stem and the constitutive relationship. *J. Anhui Agric. Sci.* **2014**, *42*, 12749–12751.
30. Zhang, J.Y. Comparative study of half-power bandwidth method and time-domain attenuation method for damping ratio solution. *Agri. Equip. Veh. Eng.* **2020**, *58*, 113–115.